# Supporting Information:

# Protein backbone motions from combined $^{13}C'$ and $^{15}N$ solid state NMR relaxation measurements

Jonathan M. Lamley,[a] Matthew J. Lougher,[a] Hans Juergen Sass,[b] Marco Rogowski,[b] Stephan Grzesiek,[b] Józef R. Lewandowski[a]

[a]Department of Chemistry, University of Warwick, Coventry CV4 7AL, UK, [b]Biozentrum, University Basel, 4056 Basel, Switzerland.

## 1. Spectral densities

### 1.1 Solution spectral densities

(a) Simple model free (SMF):[1]

$$J(\omega) = (1 - S_f^2)\frac{\tau}{1+(\omega\tau)^2} + S_f^2\frac{\tau_R^{eff}}{1+(\omega\tau_R^{eff})^2},\ \frac{1}{\tau} = \frac{1}{\tau_f} + \frac{1}{\tau_R^{eff}} \quad (1)$$

$S_f^2$ is the order parameter for internal motion, $\tau_f$ is the correlation time for internal motion and $\tau_R^{eff}$ is the correlation time for the overall rotational diffusion.

(b) Extended model free (EMF):[2]

$$J(\omega) = S_f^2 S_s^2\frac{\tau_R^{eff}}{1+(\omega\tau_R^{eff})^2} + (1 - S_f^2)\frac{\tau_f'}{1+(\omega\tau_f')^2} + S_f^2(1 - S_s^2)\frac{\tau_s'}{1+(\omega\tau_s')^2},\ \frac{1}{\tau_s'} = \frac{1}{\tau_s} + \frac{1}{\tau_R^{eff}},\ \frac{1}{\tau_f'} = \frac{1}{\tau_f} + \frac{1}{\tau_R^{eff}}, \quad (2)$$

$S_f^2$ is the order parameter for fast internal motion, $S_s^2$ is the order parameter for slow internal motion, $\tau_f$ is the correlation time for fast internal motion, $\tau_s$ is the correlation time for slow internal motion and $\tau_R^{eff}$ is the correlation time for the overall rotational diffusion.

### 1.2 Solid state spectral densities

(a) Simple model free (SMF) – motion modeled using single time scale ( $\tau_{eff}$) and amplitude ( $S^2$) of isotropic motion:[3]

$$J(\omega) = (1 - S^2)\frac{\tau_{eff}}{1+(\omega\tau_{eff})^2} \quad (3)$$

(b) Extended model free (EMF) – motion modeled using fast ( $\tau_f$, $S_f^2$) and slow ( $\tau_s$, $S_s^2$) isotropic motions:[4]

$$J(\omega) = (1 - S_f^2)\frac{\tau_f}{1+(\omega\tau_f)^2} + S_f^2(1 - S_s^2)\frac{\tau_s}{1+(\omega\tau_s)^2} \quad (4)$$

## 2. Relaxation rates

### 2.2 Spin-lattice relaxation

The rank for the spectral density indicated with subscript is retained for record keeping purposes. With the models considered below the subscript can be omitted, as the different rank spectral densities are the same.

(a) Dipolar $^1$H-$^{15}$N dipolar contribution to $^{15}$N $R_1$:

$$R_{1,NH} = \frac{1}{10}\left(\frac{\mu_0}{2\pi}\frac{\hbar\gamma_H\gamma_N}{r_{NH}^3}\right)^2 (J_0(\omega_H - \omega_N) + 3J_1(\omega_N) + 6J_2(\omega_H + \omega_N)) \quad (5)$$

*Assumptions*: We consider contribution from the directly bonded proton and the nearby non-directly bonded protons. The effective distance[5] for non-directly bonded protons contribution was on average estimated to be ~1.8 Å.

(b) CSA contribution to $^{15}$N $R_1$:

$$R_{1,NCSA} = \frac{2}{15}\omega_N^2(\sigma_{11}^2 + \sigma_{22}^2 + \sigma_{33}^2 - \sigma_{11}\sigma_{22} - \sigma_{11}\sigma_{33} - \sigma_{22}\sigma_{33})J_1(\omega_N) \quad (6)$$

*$^{15}N$ CSA:* $\sigma_{11} > \sigma_{22} > \sigma_{33}$. The components were parameterized using nitrogen isotropic chemical shift based on linear fits of the CSA components versus isotropic chemical shift for solid-state NMR CSA measurements on crystalline GB1.[6] The values are given in Table S2.

(c) CSA contribution to $^{13}C'$ $R_1$.

$$R_{1,C',CSA} = \frac{2}{15}\omega_C^2\left(\sigma_{11}^2 + \sigma_{22}^2 + \sigma_{22}^2 - \sigma_{11}\sigma_{22} - \sigma_{11}\sigma_{33} - \sigma_{22}\sigma_{33}\right)J_1(\omega_C) \quad (7)$$

$^{13}C'$ CSA: $\sigma_{11} > \sigma_{22} > \sigma_{33}$. The components were parameterized using carbonyl isotropic chemical shift based on linear fits of the CSA components versus isotropic chemical shift for solid-state NMR CSA measurements on crystalline GB1 and are given in Table S2.[7]

(d) Dipolar $^{13}C$-$^{13}C$ contribution to $^{13}C'$ $R_1$:

$$R_{1,C'C\alpha} = \frac{1}{10}\left(\frac{\mu_0}{2\pi}\frac{\hbar\gamma_C\gamma_C}{r_{C'C\alpha}^3}\right)^2 (J_0(\omega_{C'} - \omega_{C\alpha}) + 3J_1(\omega_{C'}) + 6J_2(\omega_{C'} + \omega_{C\alpha})) \quad (8)$$

*Assumptions*: $J_0(\omega_{C'} - \omega_{C\alpha})$ was evaluated at a frequency corresponding to 120 ppm for $^{13}C$.

(e) Dipolar $^{1}H$-$^{13}C$ contribution to $^{13}C'$ $R_1$:

$$R_{1,C'H} = \frac{1}{10}\left(\frac{\mu_0}{2\pi}\frac{\hbar\gamma_H\gamma_C}{r_{C'H}^3}\right)^2 (J_0(\omega_H - \omega_C) + 3J_1(\omega_C) + 6J_2(\omega_H + \omega_C)) \quad (9)$$

*Assumptions:* We considered directly contribution from amide proton and the contribution from non-directly bonded protons. The effective distance[5] for non-directly bonded protons contribution was on average estimated to be ~1.82 Å.

(f) Dipolar $^{13}C'$-$^{15}N$ contribution to $^{13}C'$ $R_1$:

$$R_{1,C'N} = \frac{1}{10}\left(\frac{\mu_0}{2\pi}\frac{\hbar\gamma_C\gamma_N}{r_{C'N}^3}\right)^2 (J_0(\omega_C - \omega_N) + 3J_1(\omega_C) + 6J_2(\omega_C + \omega_N)) \quad (10)$$

(g) Dipolar $^{13}C\alpha$-$^{15}N$ contribution to $^{15}N$ $R_1$:

$$R_{1,C\alpha N} = \frac{1}{10}\left(\frac{\mu_0}{2\pi}\frac{\hbar\gamma_C\gamma_N}{r_{C\alpha N}^3}\right)^2 (J_0(\omega_C - \omega_N) + 3J_1(\omega_N) + 6J_2(\omega_C + \omega_N)) \quad (11)$$

**2.3 Spin-lattice relaxation rate in the rotating frame**

(a) Dipolar contribution to $^{15}N$ $R_{1\rho}$:

$$R_{1\rho,NH} = \frac{1}{20}\left(\frac{\mu_0}{2\pi}\frac{\hbar\gamma_H\gamma_N}{r_{NH}^3}\right)^2 (4J_0(\omega_1) + 3J_1(\omega_N) + J_0(\omega_H - \omega_N) + 6J_1(\omega_H) + 6J_2(\omega_H + \omega_N)) \quad (12)$$

*Assumptions*: We also investigated the influence of non-directly bonded protons. The effective distance[5] for such contributions was on average estimated to be 1.8 Å. The order parameter was assumed to be the same as for NH.

(b) CSA contribution to $^{15}N$ $R_{1\rho}$:

$$R_{1\rho,N,CSA} = \frac{1}{45}\left(\sigma_{11}^2 + \sigma_{22}^2 + \sigma_{33}^2 - \sigma_{11}\sigma_{22} - \sigma_{11}\sigma_{33} - \sigma_{22}\sigma_{33}\right)\left(4J_0(\omega_1) + 3J_1(\omega_N)\right) \quad (13)$$

(c) CSA contribution to $^{13}$C' $R_{1\rho}$.

$$R_{1\rho,C',CSA} = \frac{1}{45}\omega_C^2\left(\sigma_{11}^2 + \sigma_{22}^2 + \sigma_{33}^2 - \sigma_{11}\sigma_{22} - \sigma_{11}\sigma_{33} - \sigma_{22}\sigma_{33}\right)\left(4J_0(\omega_1) + 3J_1(\omega_C)\right) \quad (14)$$

(d) Dipolar $^{13}$C-$^{13}$C contribution to $^{13}$C' $R_{1\rho}$.

$$R_{1\rho,C'C\alpha} = \frac{1}{20}\left(\frac{\mu_0}{2\pi}\frac{\hbar\gamma_C\gamma_C}{r_{C'C\alpha}^3}\right)^2 (4J_0(\omega_1) + J_0(\omega_{C'} - \omega_{C\alpha}) + 9J_1(\omega_C) + 6J_2(2\omega_C)) \quad (15)$$

*Assumptions*: $J_0(\omega_{C'} - \omega_{C\alpha})$was evaluated at a frequency corresponding to 120 ppm for $^{13}$C.

(e) Dipolar $^{1}$H-$^{13}$C contribution to $^{13}$C' $R_{1\rho}$.

$$R_{1\rho,C'H} = \frac{1}{20}\left(\frac{\mu_0}{2\pi}\frac{\hbar\gamma_C\gamma_H}{r_{C'H}^3}\right)^2 (4J_0(\omega_1) + 3J_1(\omega_C) + J_0(\omega_H - \omega_{C\alpha}) + 6J_1(\omega_H) + 6J_2(\omega_H + \omega_C)) \quad (16)$$

*Assumptions:* We also investigated the influence of non-directly bonded protons. The effective distance[5] for such contributions was on average estimated to be ~1.82 Å.

(f) Dipolar $^{13}$C'-$^{15}$N contribution to $^{13}$C' $R_{1\rho}$:

$$R_{1\rho,C'N} = \frac{1}{20}\left(\frac{\mu_0}{2\pi}\frac{\hbar\gamma_C\gamma_N}{r_{C'N}^3}\right)^2 (4J_0(\omega_1) + 3J_1(\omega_C) + J_0(\omega_C - \omega_N) + 6J_1(\omega_N) + 6J_2(\omega_N + \omega_C)) \quad (17)$$

(g) Dipolar $^{13}$Cα-$^{15}$N contribution to $^{15}$N $R_{1\rho}$:

$$R_{1\rho,C\alpha N} = \frac{1}{20}\left(\frac{\mu_0}{2\pi}\frac{\hbar\gamma_C\gamma_N}{r_{C\alpha N}^3}\right)^2 (4J_0(\omega_1) + 3J_1(\omega_N) + J_0(\omega_C - \omega_N) + 6J_1(\omega_C) + 6J_2(\omega_N + \omega_C)) \quad (18)$$

**Table S2.** Relaxation-active interactions in the peptide plane frame. The $^{15}$N and $^{13}$C' CSA components were parameterized using linear fits of the CSA components versus isotropic chemical shift for solid-state NMR CSA measurements on crystalline GB1.[6,7]

| Relaxation active interaction | Geometrical and CSA parameters |
|---|---|
| $^{15}$N-H | 1.02Å |
| $^{15}$N-CSA | $\sigma_{11}$=1.1283$\sigma_{iso}$+93.77 (ppm)[6]<br>$\sigma_{22}$=1.0086$\sigma_{iso}$ -42.475 (ppm)[6]<br>$\sigma_{33}$=0.8631$\sigma_{iso}$ -51.295 (ppm)[6] |
| 15N-13C′ | 1.33 Å |
| 15N-13Cα | 1.46 Å |
| 13C′-13C$^{\alpha}$ | 1.525 Å |
| $^{13}$C′-H$^{N}$ | 2.04 Å |
| $^{13}$C′-CSA | $\sigma_{11}$=0.24$\sigma_{iso}$+200 (ppm)[7]<br>$\sigma_{22}$=2.82$\sigma_{iso}$ –305 (ppm)[7]<br>$\sigma_{33}$=96.5 (ppm)[7] |

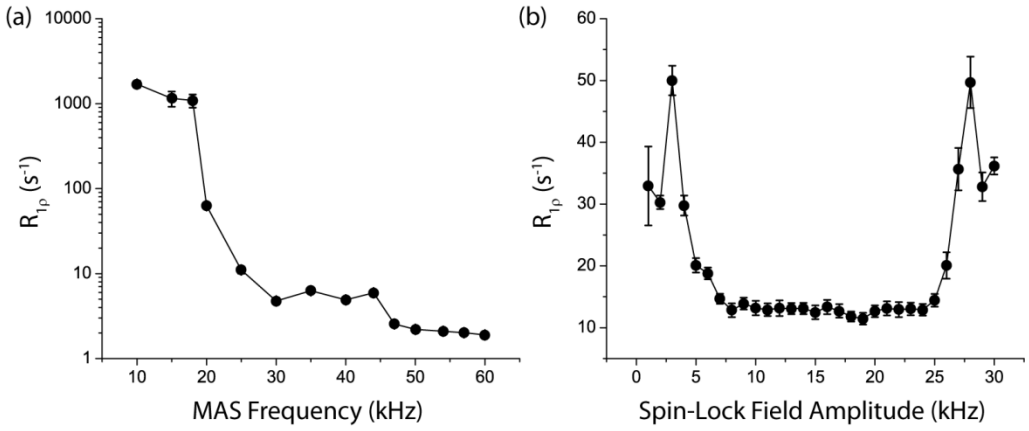


**Figure S1**. Bulk carbonyl $^{13}$C $R_{1\rho}$ in [U-$^{13}$C, $^{15}$N]GB1, measured as a function of (a) magic angle spinning (MAS) frequency (with a constant spin-lock amplitude of 17 kHz), and (b) spin-lock field amplitude (with a constant MAS frequency of 60 kHz) at a field of 14.1 T (600 MHz $^{1}$H Larmor frequency). Sample temperature was 27 °C for all experiments, as determined by the chemical shift of water with respect to DSS. Rates were found in 1D by measuring total carbonyl peak integrals at incrementally longer spin-lock pulses. The $^{13}$C spin-lock fields were calibrated from nutation experiments. $^{13}$C $R_{1\rho}$ rates clearly plateau at spinning frequencies greater than ~45 kHz and above spin-lock nutation frequencies above ~8 kHz, avoiding recoupling conditions such as HORROR ($\omega_1 = \omega_r/2$) where anisotropic interactions may be reintroduced (e.g. close to 30 kHz spin-lock amplitude in (b)). Note that the GB1 sample used for these measurements was of a different crystalline form to the sample used for the site-specific measurements presented in the manuscript (and in Table S1), yielding somewhat higher average values for $^{13}$C $R_{1\rho}$ under the same experimental conditions.

## Magic angle mis-adjustment

As magic angle spinning plays a crucial role in averaging the interactions contributing to the coherent mechanisms for the magnetization decay, it is important to consider the influence of "mis-setting" the magic angle upon the efficiency of averaging by MAS. We examine the effect of mis-setting the angle of rotation on the measured coherence lifetimes in [1-$^{13}$C]Ala in Fig. S2, where the measured $R_{1\rho}$ rates for $^{13}$C' are plotted as a function of the $^{13}$C' line width measured in a cross-polarization (CP) experiment. At the magic angle (~54.736°) the $^{13}$C' line width was ~21 Hz, and from here the angle was systematically mis-adjusted up to a setting that yielded a $^{13}$C' line width of 54 Hz. In the explored range we found that the measured $R_{1\rho}$ changed by less than 2%, suggesting that the $R_{1\rho}$ measurement is relatively forgiving to a slight mis-adjustment of the magic angle.

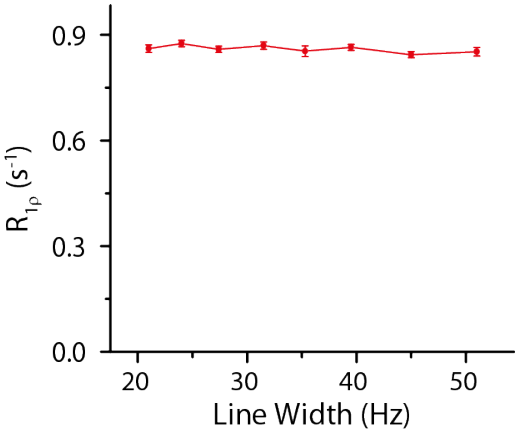


**Figure S2**. $^{13}$C' $R_{1\rho}$ in [1-$^{13}$C]alanine as a function of deviation of the rotor axis from the magic angle. The horizontal axis depicts $^{13}$C' line width, itself a function of the rotor angle setting; 21 Hz corresponds to a "well-set" magic angle, while larger line width indicates larger deviation from the magic angle. Measurements were performed at $\omega_{0H}/2\pi$ = 600 MHz, $\omega_r/2\pi$ = 60 kHz and $\omega_1/2\pi$ = 17 kHz.

## Temperature effects

The $^{13}$C' $R_{1\rho}$ experiment is relatively robust with respect to sample temperature changes (from r.f.-induced heating) during the spin-lock pulse. We measured the temperature change of the GB1 sample (50 mM salt, pH 5.5) at $\omega_{0H}/2\pi$ = 600 MHz upon application of a $^{13}$C spin-lock pulse prior to acquisition. The temperature was measured based on the chemical shift of water protons (a Bruker au macro for calculating the temperature of the sample based on the chemical shift of water with respect to an internal DSS reference, including effects of pH and salt concentration, can be downloaded from http://www2.warwick.ac.uk/fac/sci/chemistry/research/lewandowski/lewandowskigroup/goodies/). For reference, the sample temperature without any $^{13}$C irradiation was 26.9 ± 0.5 °C. A total of 50 experiments with 0.3 s of 17 kHz spin-lock irradiation were performed (32 scans per experiment with a recycle delay of 2 s, resulting in a total time for each experiment of ~74 s) back to back, for a total of ~62 minutes. The measured sample temperature had increased by 1.5 ± 0.5 °C after a single experiment, but then remained at a constant 28.4 ± 0.5 °C for the remainder of the 62 minute run, showing that equilibrium is reached quickly (a few transients) without the long stabilization time observed for larger rotors at slower spinning frequencies and under the application of high power heteronuclear decoupling. As 0.3 s is at the limit of what must typically be sampled experimentally (we sampled to 0.2 s at 17 kHz for $^{13}$C, plus a combined 50 ms of 15 kHz slpTPPM decoupling during $t_1$ and $t_2$ acquisition periods), internal sample temperatures should not be expected to exceed a temperature 1.5 °C higher than equilibrium at any point during an $R_{1\rho}$ experiment. To examine the relationship between temperature increase and spin-lock pulse length under typical experimental conditions (60 kHz MAS, 17 kHz spin-lock field strength), further test experiments were conducted with spin-lock pulses ranging from 10 μs to 300.01 ms (see Fig. S3). Naturally, the sample was observed to increase in temperature with increased pulse length, but at a rate of just ~0.005 K ms$^{-1}$ (assuming a linear relationship). The difference in sample temperature between different spin-lock lengths sampled is clearly very small (maximum of 1.5 °C dif-

ference between shortest and longest spin-lock pulses employed in an experiment) and for most purposes may be considered negligible. Temperature changes between experiments with different spin-lock times may be minimized by employing a "constant heating time" version of experiment, where an additional spin–lock pulse is applied after acquisition in order to keep the overall length of the spin lock pulse constant.

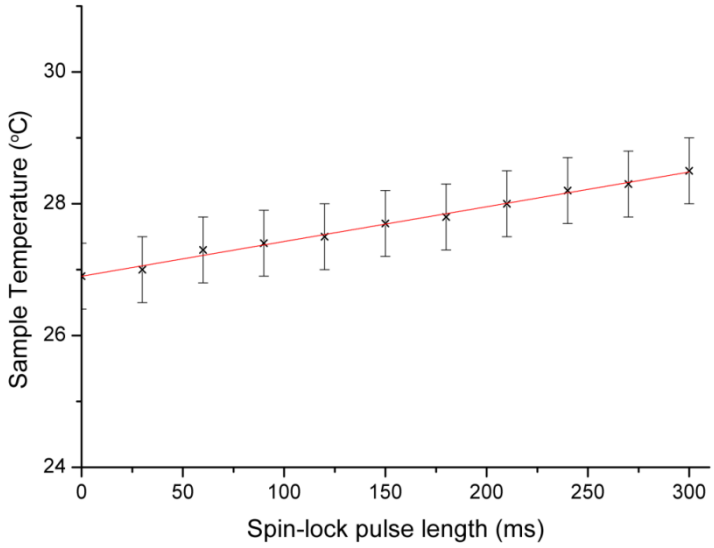


**Figure S3.** Sample temperature as a function of spin-lock pulse length, as measured by the chemical shift of water protons with respect to internal DSS in a sample of [U-$^{13}$C,$^{15}$N]GB1 (50 mM salt concentration, pH 5.5).[8,9] Experiments were measured at 14.1 T at 60 kHz MAS frequency, with a spin-lock nutation frequency of 17 kHz (corresponding to 2.49 W) and the initial (i.e. in the absence of spin-lock) sample temperature of 26.9 ± 0.5 °C.

These results also illustrate that the technology employed here provides a practical and safe approach for measuring relaxation dispersion for spin-lock frequencies in the range from ~1 kHz to a few tens of kHz (or more if the length of spin-lock is limited to a few tens of milliseconds), which significantly expands the range of time scales accessible with such methodology to a few microseconds, and complementing CPMG in perdeuterated proteins[10]. Relaxation dispersion in the solid state could potentially be highly complementary to similar measurements in solution, where currently even with cryo-cooled NMR probe heads the current limit for safe spin-lock field strengths is ~6.4 kHz (corresponding to a minimum detectable time scale of $1/(2\pi*6.4\text{ kHz}) \approx 25\ \mu s$).[11]

## Polarization transfer

Another potential complication associated with carbonyl $R_{1\rho}$ experiments is that of polarization transfer between different sites during the spin-lock pulse, namely via isotropic mixing or r.f.-driven spin diffusion mechanisms. In the solution state it has been noted that evolution under homonuclear three-bond scalar couplings can lead to magnetization transfer during spin-locking ("isotropic mixing") between carbonyls of neighboring residues whose resonances are close in chemical shift, leading to inaccurate $R_{1\rho}$ measurements.[12] To check that neither this nor r.f.-driven spin diffusion would compromise our solid-state experiments, we ran a 2D $^{13}$C-$^{13}$C experiment (on-resonance with $^{13}$C') with a "mixing" block (between $t_1$ and $t_2$ acquisition) consisting of a 150 ms, 17 kHz spin-lock pulse. After a total of 56 scans (~14.5 hours) no off-diagonal cross-peaks were observed above the noise level (spectrum in Fig. S4) between carbonyls (or between $^{13}$C' and $^{13}C_\alpha$), suggesting that neither mechanism is efficient for polarization transfer under the employed conditions. Note, however, that r.f.-driven spin diffusion may become more of a concern for aliphatic carbons.

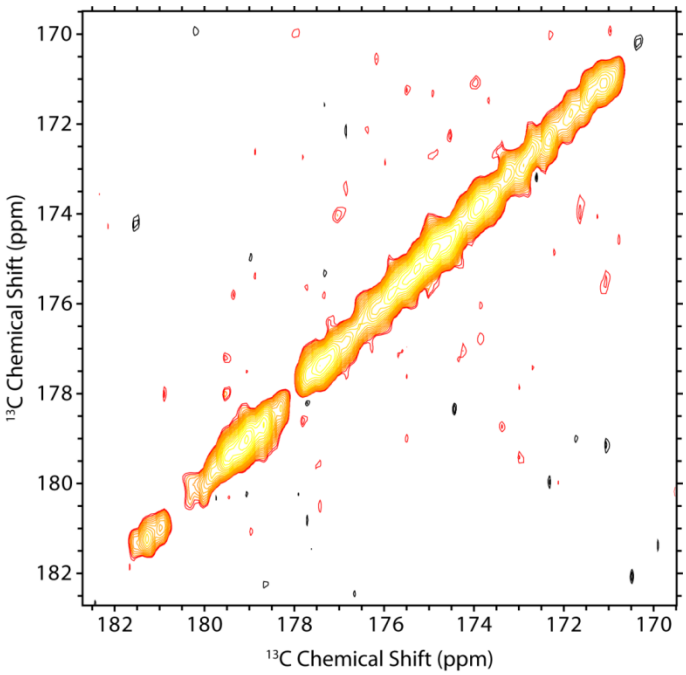


**Figure S4.** Spectrum resulting from an experiment to test for the occurrence of isotropic mixing and r.f.-driven spin diffusion during a spin-lock pulse typical of that employed in a $^{13}$C' $R_{1\rho}$ experiment. After a 150 ms "mixing" block of 17 kHz $^{13}$C' irradiation, no $^{13}$C'-$^{13}$C' cross-peaks are seen above the level of noise (negative contours in black, positive in red-yellow), implying little or no polarization transfer occurs.

**Table S3.** Summary of measured carbonyl $^{13}C$ and amide $^{15}N$ $R_{1\rho}$ and $R_1$ rates in [U-$^{13}C$,$^{15}N$]GB1 at fields of 14.1 T and 20.0 T ($^1H$ Larmor frequencies of 600 MHz and 850 MHz respectively). $^{13}C$ and $^{15}N$ $R_{1\rho}$ and $R_1$ rates were measured with the pulse sequences shown in Figure S10, at a sample temperature of 27 ± 2 °C.

| | **600 MHz** | | | | **850 MHz** | | | |
|---|---|---|---|---|---|---|---|---|
| *Residue* | $^{13}C'$ $R_{1\rho}$ *(s$^{-1}$)* | $^{13}C'$ $R_1$ *(s$^{-1}$)* | $^{15}N$ $R_{1\rho}$ *(s$^{-1}$)* | $^{15}N$ $R_1$ *(s$^{-1}$)* | $^{13}C'$ $R_{1\rho}$ *(s$^{-1}$)* | $^{13}C'$ $R_1$ *(s$^{-1}$)* | $^{15}N$ $R_{1\rho}$ *(s$^{-1}$)* | $^{15}N$ $R_1$ *(s$^{-1}$)* |
| 1 | 2.48 ± 0.28 | 0.11 ± 0.01 | – | – | 4.50 ± 0.64 | 0.09 ± 0.01 | – | – |
| 2 | 0.98 ± 0.27 | 0.14 ± 0.05 | 1.59 ± 0.24 | 0.050 ± 0.008 | 2.21 ± 0.74 | 0.13 ± 0.01 | 1.28 ± 0.23 | 0.106 ± 0.029 |
| 3 | 2.41 ± 0.53 | 0.16 ± 0.02 | 1.92 ± 0.23 | 0.039 ± 0.007 | 4.10 ± 0.72 | 0.17 ± 0.02 | 1.34 ± 0.41 | 0.053 ± 0.021 |
| 4 | 2.89 ± 0.54 | 0.22 ± 0.04 | 1.31 ± 0.12 | 0.013 ± 0.007 | 3.81 ± 0.31 | 0.14 ± 0.01 | 0.88 ± 0.31 | 0.009 ± 0.006 |
| 5 | 0.94 ± 0.32 | 0.17 ± 0.03 | 1.72 ± 0.1 | 0.030 ± 0.006 | 1.65 ± 0.37 | 0.24 ± 0.06 | 1.72 ± 0.38 | 0.029 ± 0.006 |
| 6 | 1.59 ± 0.40 | 0.14 ± 0.04 | 0.82 ± 0.21 | 0.023 ± 0.007 | 2.46 ± 0.45 | 0.23 ± 0.06 | 0.73 ± 0.20 | 0.008 ± 0.013 |
| 7 | 2.48 ± 0.43 | 0.30 ± 0.09 | 0.65 ± 0.23 | 0.016 ± 0.004 | 2.94 ± 0.64 | 0.34 ± 0.08 | 0.76 ± 0.1 | 0.023 ± 0.007 |
| 8 | 2.60 ± 0.28 | 0.55 ± 0.06 | 0.97 ± 0.23 | 0.020 ± 0.003 | 4.58 ± 0.62 | 0.39 ± 0.03 | 0.91 ± 0.24 | 0.021 ± 0.005 |
| 9 | 2.82 ± 0.66 | 0.13 ± 0.02 | 1.00 ± 0.15 | 0.031 ± 0.005 | 6.84 ± 1.52 | 0.14 ± 0.01 | 2.03 ± 0.37 | 0.051 ± 0.012 |
| 10 | 4.28 ± 0.52 | 0.18 ± 0.02 | 1.54 ± 0.49 | 0.088 ± 0.023 | 7.09 ± 0.75 | 0.15 ± 0.01 | 3.44 ± 0.58 | 0.058 ± 0.014 |
| 11 | 5.77 ± 0.43 | 0.20 ± 0.03 | 3.86 ± 0.35 | 0.060 ± 0.004 | 14.6 ± 2.9 | 0.22 ± 0.02 | 8.33 ± 0.96 | 0.131 ± 0.040 |
| 12 | 1.50 ± 0.40 | 0.25 ± 0.06 | 3.36 ± 0.32 | 0.048 ± 0.006 | 3.87 ± 0.76 | 0.26 ± 0.03 | 7.58 ± 0.99 | 0.076 ± 0.033 |
| 13 | 6.34 ± 0.64 | 0.24 ± 0.03 | 1.05 ± 0.18 | 0.027 ± 0.007 | 6.30 ± 0.74 | 0.20 ± 0.01 | 1.95 ± 0.14 | 0.026 ± 0.016 |
| 14 | 2.81 ± 0.66 | 0.09 ± 0.02 | 1.26 ± 0.30 | 0.037 ± 0.004 | 4.40 ± 0.74 | 0.09 ± 0.01 | 2.39 ± 0.34 | 0.035 ± 0.011 |
| 15 | 3.26 ± 0.38 | 0.21 ± 0.03 | 0.86 ± 0.24 | 0.031 ± 0.012 | 2.87 ± 0.44 | 0.17 ± 0.01 | 1.52 ± 0.38 | 0.045 ± 0.008 |
| 16 | 6.80 ± 0.62 | 0.16 ± 0.02 | 1.42 ± 0.29 | 0.039 ± 0.007 | 5.66 ± 0.58 | 0.12 ± 0.01 | 1.43 ± 0.26 | 0.031 ± 0.017 |
| 17 | 6.56 ± 1.26 | 0.22 ± 0.02 | 5.94 ± 0.62 | 0.065 ± 0.016 | 9.69 ± 0.67 | 0.15 ± 0.01 | 4.27 ± 0.39 | 0.127 ± 0.052 |
| 18 | 2.35 ± 0.29 | 0.12 ± 0.01 | 3.86 ± 0.44 | 0.059 ± 0.013 | 3.88 ± 0.75 | 0.11 ± 0.01 | 3.00 ± 0.35 | 0.058 ± 0.011 |
| 19 | 3.21 ± 0.31 | 0.14 ± 0.01 | 0.70 ± 0.15 | 0.066 ± 0.009 | 3.51 ± 0.73 | 0.12 ± 0.01 | 0.92 ± 0.29 | 0.064 ± 0.008 |
| 20 | 3.39 ± 0.55 | 0.14 ± 0.02 | 2.22 ± 0.34 | 0.060 ± 0.006 | 5.10 ± 0.54 | 0.07 ± 0.02 | 2.83 ± 0.34 | 0.111 ± 0.007 |
| 21 | 5.21 ± 0.69 | 0.10 ± 0.02 | 1.92 ± 0.17 | 0.043 ± 0.006 | 5.14 ± 0.63 | 0.10 ± 0.01 | 2.99 ± 0.43 | 0.066 ± 0.019 |
| 22 | 2.75 ± 0.50 | 0.09 ± 0.01 | 2.31 ± 0.38 | 0.064 ± 0.017 | 4.28 ± 0.44 | 0.11 ± 0.01 | 4.41 ± 0.53 | 0.106 ± 0.035 |
| 23 | 1.87 ± 0.23 | 0.20 ± 0.03 | 1.78 ± 0.24 | 0.022 ± 0.005 | 3.77 ± 0.65 | 0.19 ± 0.04 | 2.17 ± 0.44 | 0.045 ± 0.011 |
| 24 | 3.89 ± 0.59 | 0.16 ± 0.03 | 0.89 ± 0.11 | 0.031 ± 0.004 | 3.33 ± 1.20 | 0.14 ± 0.01 | 2.04 ± 0.20 | 0.056 ± 0.017 |
| 25 | 2.34 ± 0.25 | 0.16 ± 0.02 | 3.37 ± 0.37 | 0.017 ± 0.011 | 2.73 ± 0.39 | 0.13 ± 0.01 | 5.08 ± 1.12 | 0.009 ± 0.023 |
| 26 | 2.77 ± 0.33 | 0.40 ± 0.07 | 0.91 ± 0.18 | 0.015 ± 0.008 | 2.90 ± 0.71 | 0.26 ± 0.06 | 1.55 ± 0.22 | 0.060 ± 0.033 |
| 27 | 2.01 ± 0.32 | 0.16 ± 0.05 | 0.51 ± 0.16 | 0.026 ± 0.009 | 3.16 ± 0.75 | 0.25 ± 0.03 | 1.18 ± 0.17 | 0.021 ± 0.009 |
| 28 | 1.53 ± 0.29 | 0.38 ± 0.12 | 1.25 ± 0.23 | 0.026 ± 0.005 | 2.34 ± 0.75 | 0.36 ± 0.10 | 1.89 ± 0.44 | 0.024 ± 0.012 |
| 29 | 1.10 ± 0.23 | 0.25 ± 0.04 | 1.60 ± 0.23 | 0.028 ± 0.004 | 3.30 ± 0.30 | 0.13 ± 0.03 | 1.27 ± 0.32 | 0.022 ± 0.009 |
| 30 | 2.61 ± 0.63 | 0.06 ± 0.01 | 1.16 ± 0.17 | 0.018 ± 0.004 | 3.16 ± 0.60 | 0.07 ± 0.02 | 1.47 ± 0.26 | 0.029 ± 0.012 |
| 31 | 1.54 ± 0.13 | 0.20 ± 0.04 | 0.83 ± 0.17 | 0.009 ± 0.004 | 1.10 ± 0.53 | 0.12 ± 0.02 | 1.14 ± 0.36 | 0.026 ± 0.008 |
| 32 | 1.88 ± 0.35 | 0.25 ± 0.08 | 0.89 ± 0.08 | 0.026 ± 0.003 | 2.63 ± 0.24 | 0.18 ± 0.03 | 1.32 ± 0.17 | 0.030 ± 0.011 |
| 33 | 2.01 ± 0.35 | 0.79 ± 0.21 | 0.62 ± 0.25 | 0.005 ± 0.007 | 2.83 ± 0.44 | 0.50 ± 0.06 | 0.78 ± 0.25 | 0.020 ± 0.015 |

| | 600 MHz | | | | 850 MHz | | | |
|---|---|---|---|---|---|---|---|---|
| *Residue* | $^{13}C'$ $R_{1\rho}$ ($s^{-1}$) | $^{13}C'$ $R_1$ ($s^{-1}$) | $^{15}N$ $R_{1\rho}$ ($s^{-1}$) | $^{15}N$ $R_1$ ($s^{-1}$) | $^{13}C'$ $R_{1\rho}$ ($s^{-1}$) | $^{13}C'$ $R_1$ ($s^{-1}$) | $^{15}N$ $R_{1\rho}$ ($s^{-1}$) | $^{15}N$ $R_1$ ($s^{-1}$) |
| 34 | 1.30 ± 0.19 | 0.31 ± 0.09 | 0.93 ± 0.19 | 0.008 ± 0.005 | 1.99 ± 0.37 | 0.31 ± 0.07 | 0.83 ± 0.30 | 0.005 ± 0.02 |
| 35 | 1.65 ± 0.08 | 0.18 ± 0.03 | 0.47 ± 0.16 | 0.022 ± 0.009 | 2.79 ± 0.15 | 0.17 ± 0.03 | 0.96 ± 0.33 | 0.021 ± 0.014 |
| 36 | 3.82 ± 0.67 | 0.30 ± 0.06 | 0.88 ± 0.08 | 0.021 ± 0.003 | 3.97 ± 0.42 | 0.33 ± 0.04 | 1.5 ± 0.10 | 0.031 ± 0.005 |
| 37 | 3.30 ± 0.47 | 0.17 ± 0.02 | 1.23 ± 0.38 | 0.027 ± 0.006 | 3.31 ± 0.42 | 0.20 ± 0.02 | 1.01 ± 0.50 | 0.028 ± 0.010 |
| 38 | 9.85 ± 1.22 | 0.13 ± 0.02 | 1.07 ± 0.20 | 0.029 ± 0.008 | 8.48 ± 1.09 | 0.19 ± 0.04 | 1.67 ± 0.22 | 0.021 ± 0.008 |
| 39 | 3.12 ± 0.56 | 0.19 ± 0.03 | 3.00 ± 0.46 | 0.050 ± 0.020 | 5.80 ± 0.85 | 0.25 ± 0.02 | 4.62 ± 0.53 | 0.040 ± 0.017 |
| 40 | 6.14 ± 0.55 | 0.24 ± 0.04 | 3.07 ± 0.27 | 0.101 ± 0.015 | 6.82 ± 0.76 | 0.21 ± 0.02 | 4.26 ± 0.34 | 0.304 ± 0.058 |
| 41 | 2.74 ± 0.36 | 0.06 ± 0.02 | 3.22 ± 0.29 | 0.204 ± 0.058 | 2.74 ± 0.70 | 0.08 ± 0.01 | 6.04 ± 0.70 | 0.245 ± 0.039 |
| 42 | 2.85 ± 0.31 | 0.24 ± 0.07 | 1.46 ± 0.34 | 0.087 ± 0.015 | 2.92 ± 0.46 | 0.14 ± 0.03 | 2.42 ± 0.50 | 0.112 ± 0.013 |
| 43 | 5.70 ± 0.73 | 0.31 ± 0.06 | 1.27 ± 0.22 | 0.027 ± 0.009 | 4.79 ± 0.64 | 0.12 ± 0.02 | 1.68 ± 0.38 | 0.024 ± 0.016 |
| 44 | 4.00 ± 0.90 | 0.15 ± 0.02 | 1.96 ± 0.45 | 0.019 ± 0.012 | 4.96 ± 0.48 | 0.11 ± 0.01 | 1.84 ± 0.74 | 0.016 ± 0.010 |
| 45 | 3.32 ± 0.55 | 0.14 ± 0.01 | 1.62 ± 0.35 | 0.012 ± 0.009 | 3.41 ± 0.39 | 0.09 ± 0.01 | 2.02 ± 0.55 | 0.012 ± 0.014 |
| 46 | 3.20 ± 0.52 | 0.29 ± 0.05 | 0.90 ± 0.22 | 0.041 ± 0.010 | 3.71 ± 0.93 | 0.18 ± 0.02 | 1.18 ± 0.31 | 0.029 ± 0.009 |
| 47 | 2.83 ± 0.67 | 0.17 ± 0.03 | 1.17 ± 0.28 | 0.033 ± 0.006 | 4.36 ± 0.34 | 0.17 ± 0.01 | 2.06 ± 0.42 | 0.049 ± 0.021 |
| 48 | 1.83 ± 0.45 | 0.25 ± 0.03 | 1.94 ± 0.23 | 0.030 ± 0.008 | 3.58 ± 0.48 | 0.23 ± 0.02 | 3.01 ± 0.40 | 0.033 ± 0.013 |
| 49 | 2.56 ± 0.71 | 0.36 ± 0.12 | 1.06 ± 0.24 | 0.043 ± 0.004 | 2.99 ± 0.64 | 0.20 ± 0.05 | 1.72 ± 0.40 | 0.022 ± 0.009 |
| 50 | 2.06 ± 0.33 | 0.29 ± 0.08 | 1.33 ± 0.24 | 0.039 ± 0.008 | 2.38 ± 0.77 | 0.24 ± 0.06 | 1.70 ± 0.40 | 0.01 ± 0.014 |
| 51 | 2.15 ± 0.49 | 0.38 ± 0.06 | 0.58 ± 0.19 | 0.012 ± 0.005 | 2.04 ± 0.66 | 0.23 ± 0.02 | 1.26 ± 0.29 | 0.036 ± 0.016 |
| 52 | 3.13 ± 0.39 | 0.24 ± 0.07 | 0.66 ± 0.13 | 0.009 ± 0.008 | 3.91 ± 0.52 | 0.23 ± 0.03 | 1.68 ± 0.27 | 0.019 ± 0.011 |
| 53 | 5.29 ± 0.81 | 0.16 ± 0.05 | 1.90 ± 0.40 | 0.003 ± 0.005 | 7.05 ± 0.99 | 0.15 ± 0.02 | 2.88 ± 0.41 | 0.011 ± 0.007 |
| 54 | 2.14 ± 0.39 | 0.23 ± 0.08 | 3.44 ± 0.38 | 0.005 ± 0.004 | 3.12 ± 0.38 | 0.16 ± 0.03 | 5.05 ± 0.72 | 0.020 ± 0.009 |
| 55 | 3.75 ± 0.32 | 0.28 ± 0.01 | 0.79 ± 0.23 | 0.001 ± 0.009 | 5.67 ± 0.70 | 0.22 ± 0.01 | 0.85 ± 0.20 | 0.029 ± 0.011 |
| 56 | – | – | 1.65 ± 0.15 | 0.065 ± 0.011 | – | – | 2.40 ± 0.42 | 0.102 ± 0.018 |

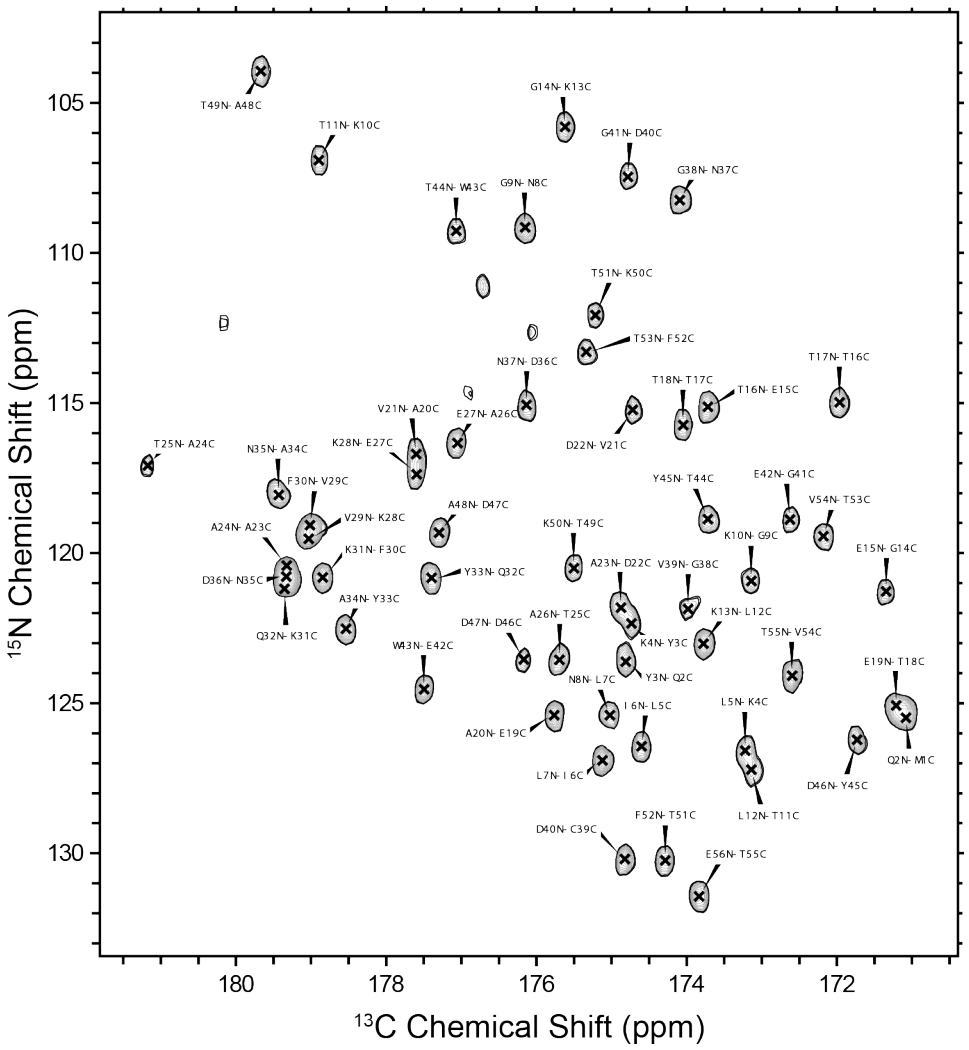


**Figure S5.** NCO $S^3E$ DCP spectrum measured at $\omega_{0H}/2\pi$ = 850 MHz showing resonance assignments. Note that a number of peaks partially overlap and as such the rates extracted from them may be distorted. Assignments are not shown for side-chain cross peaks.

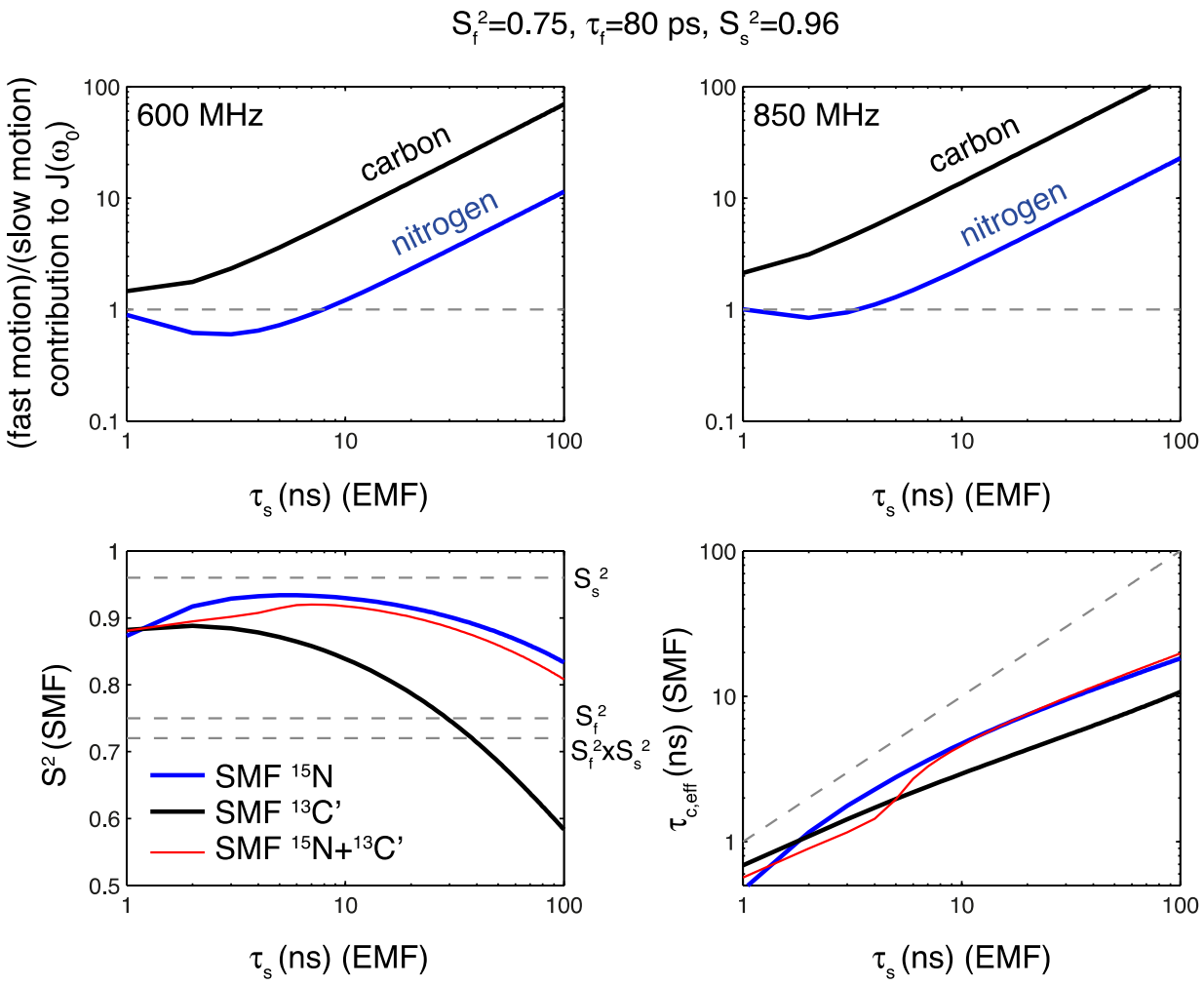


**Figure S6.** *Top panels*: Ratio of the fast motion contribution to $J_1(\omega_0)$ (with $\tau_f$ = 80 ps, $S_f^2$= 0.75) to that of a slow motion ( $S_s^2$ =0.94, $\tau_s$ indicated on the horizontal axis), calculated using SMF (Eq. 1.3) at $\omega_{0H}/2\pi$ = 600 and 850 MHz. *Bottom panels*: The result of fitting to a single timescale motion (using SMF: Eq. 1.3 and 1.7-1.18) rates simulated using two timescale motion (using EMF: Eq. 1.4 and 1.7-1.18) with the settings as in the top panels ( $S_f^2$, $S_s^2$ and $S_f^2S_s^2$ are indicated by dashed grey lines). We assumed 10% error for the simulated rates in the SMF fit. Note the offset between the order parameter for $^{15}$N and $^{13}$C' when SMF is used for modeling the data resulting from two timescale motion.

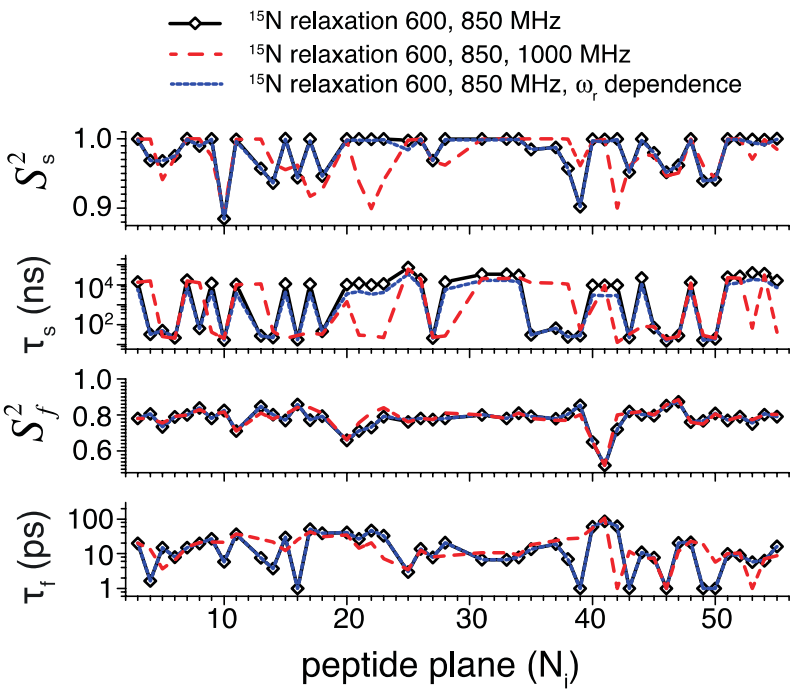


**Figure S7.** EMF analysis of backbone dynamics in crystalline GB1 based on $^{15}$N $R_1$ and $R_{1\rho}$ measurements performed at 600 and 850 MHz $^1$H Larmor frequency and $^{15}$N dipolar coupling measurements (diamond black line), compared to an analogous analysis with the addition of $^{15}$N $R_1$ and $R_{1\rho}$ measured at 1 GHz $^1$H Larmor frequency (red dashed line) and an analysis where the generalized expressions for $R_{1\rho}$ including the effect of spinning frequency[13] were used (blue dotted line). In the current case neither of these approaches leads to complete elimination of fitting artifacts.

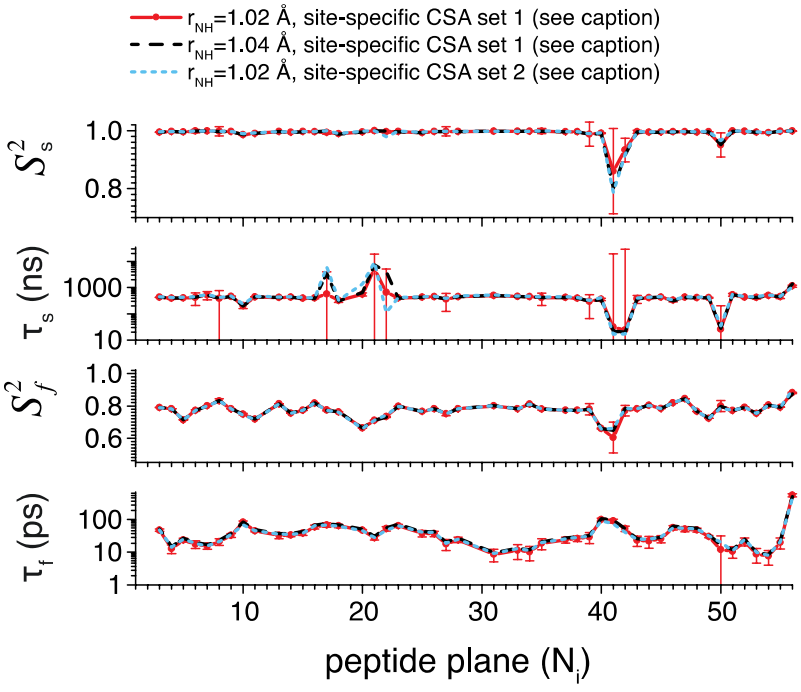


**Figure S8.** The effect of $r_{NH}$ and $^{15}$N & $^{13}$C' CSA on the results of an EMF analysis of backbone dynamics in crystalline GB1. For the fits represented by the red line, $r_{NH}$ = 1.02 Å, site specific $^{15}$N CSA from [Wylie, B. J. *et al. Proc. Natl. Acad. Sci.* 2011, 108, 16974–16979.] and site specific $^{13}$C' CSA from ref. [Wylie, B. J. *et al. J. Am. Chem. Soc.* 2007, 129, 5318–9.] were used. For the fits represented with the black line, $r_{NH}$ = 1.04 Å, site specific $^{15}$N CSA from [Wylie, B. J. *et al. Proc.*

*Natl. Acad. Sci.* 2011, 108, 16974–16979.] and site specific $^{13}$C' CSA from [Wylie, B. J. *et al. J. Am. Chem. Soc.* 2007, 129, 5318–9.] were used. For the fits represented with the blue line, $r_{NH}$ = 1.02 Å, site specific $^{15}$N/$^{13}$C' CSA from [Loth, K.; Pelupessy, P.; Bodenhausen, G. *J. Am. Chem. Soc.* 2005, 127, 6062–8.] were used. In all cases the EMF analysis was based on $^{15}$N and $^{13}$C' $R_1$ and $R_{1\rho}$ performed at 600 and 850 MHz $^1$H Larmor frequency with $^{15}$N dipolar coupling measurements used for constraining the overall amplitude of motions (assuming a rigid NH bond length of 1.02 Å). The simulations illustrate that the EMF analysis in the solid state is less sensitive to the choice of bond lengths and CSA compared to in solution.

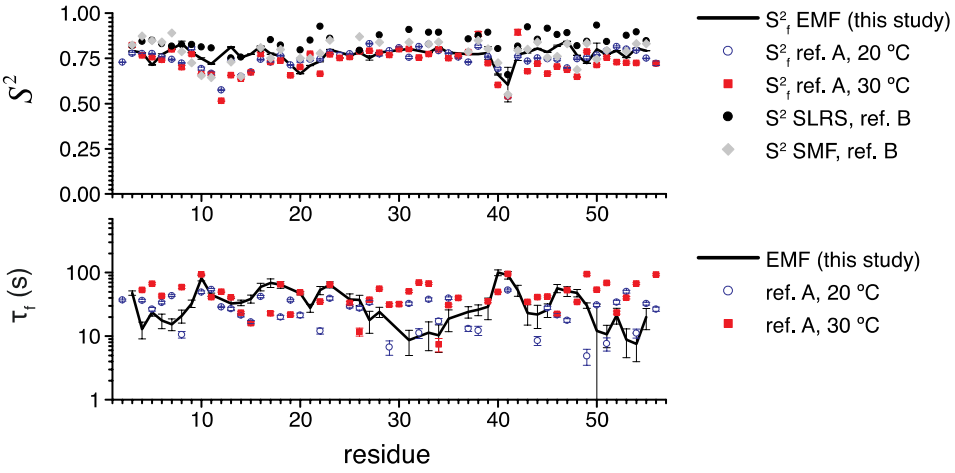


**Figure S9.** Comparison of the fast motion parameters from the EMF analysis (see Fig. 5) with various SMF analyses based on relaxation in solution. Reference A is [14]. Reference B is [15].

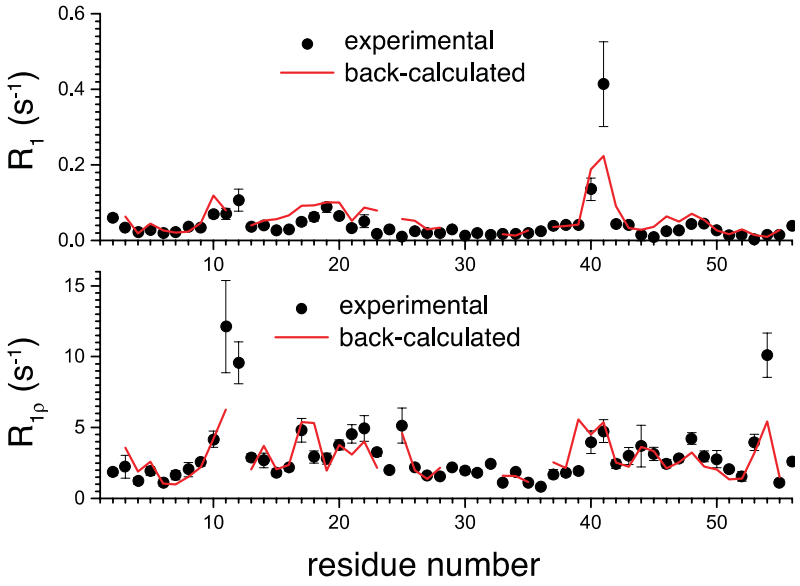


**Figure S10.** Comparison of $^{15}$N relaxation rates measured in crystalline GB1 at 1 GHz $^1$H Larmor frequency (black points) and those back-calculated from an EMF analysis based on $^{15}$N and $^{13}$C' $R_1$ and $R_{1\rho}$ measurements performed at 600 and 850 MHz $^1$H Larmor frequency with $^{15}$N dipolar coupling measurements used for constraining the overall amplitude of motions (red line).

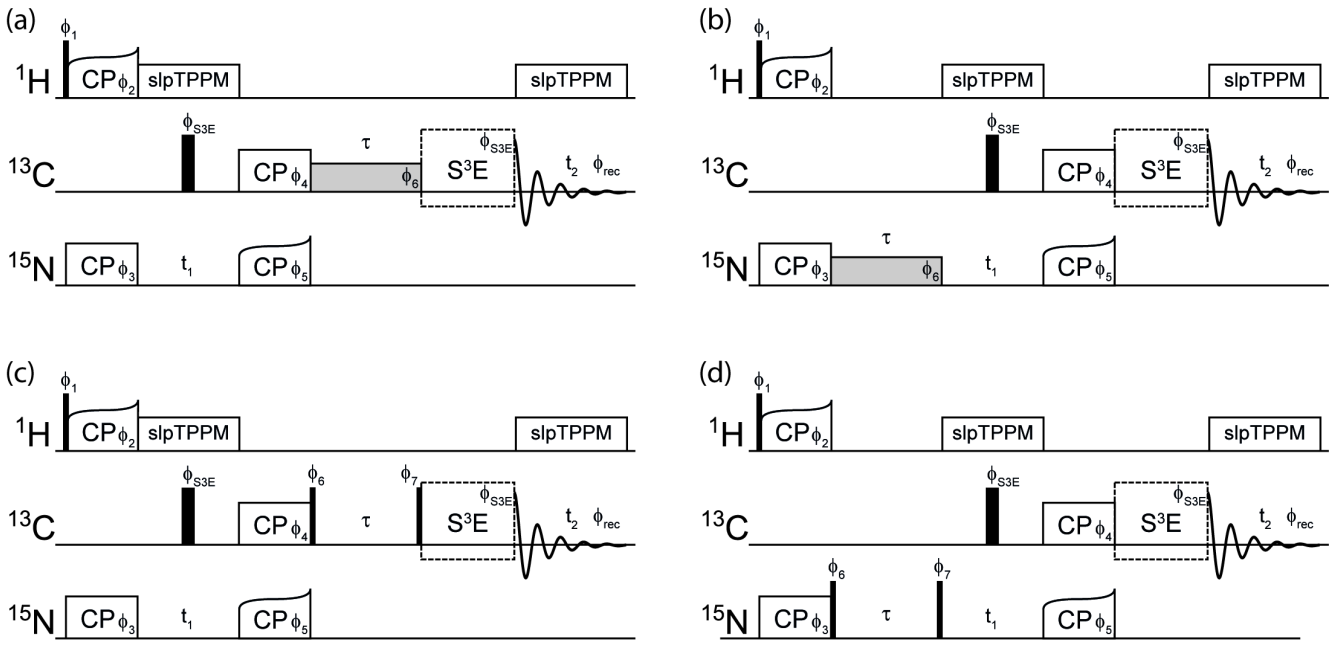


**Figure S11.** Pulse sequences for the site-specific measurement of (a) carbonyl $^{13}C$ $R_{1\rho}$, (b) amide $^{15}N$ $R_{1\rho}$, (c) carbonyl $^{13}C$ $R_1$ and (d) amide $^{15}N$ $R_1$. $^{13}C$ and $^{15}N$ frequency offsets are set to the centers of the carbonyl and amide regions respectively. Pulses with a flip angle of $\pi/2$ are indicated with a narrow black rectangle, while $\pi$ pulses are denoted by a thicker black rectangle. Spin-lock pulses (for (a) and (b)) are indicated in light grey. Indirect and direct acquisition periods are labeled as "$t_1$" and "$t_2$" respectively, while phases are shown as "$\phi$". For all sequences, slpTPPM[16] decoupling is applied on the proton channel during acquisition periods at $^1H$ amplitude of one quarter of the sample spinning frequency. Site-specific relaxation rates are obtained from curves obtained by monitoring intensity of cross peaks in 2D experiments as a function of relaxation time, $\tau$ (length of spin-lock pulse for $R_{1\rho}$ measurements, delay length for $R_1$ measurements). No $^1H$ decoupling is applied during relaxation periods. In each sequence, the rectangle with a dashed outline represents an $S^3E$ block, which may be optionally included to improve resolution in the direct dimension by minimizing the effect of one-bond C'-$C_\alpha$ J-couplings.[17] Experiments containing "A" and "B" blocks (which differ in the positioning of the band-selective pulses – see [17]) are run in an interleaved fashion, to be split and recombined when processing. The two different phase cycles associated with these are differentiated by use of square brackets below. The phases of all $S^3E$ pulses (including the $\pi$ pulse on $^{13}C$ during $t_1$ evolution) are identical, labeled as $\phi_{S3E}$. Phase cycling (with $S^3E$):

(a) $\phi_1 = (+y\ -y)$, $\phi_2 = \phi_3 = \phi_5 = \phi_{S3E} = (+x)$, $\phi_4 = \phi_6 = (+x\ +x\ -x\ -x$ [A] / $-y\ -y\ +y\ +y$ [B]), $\phi_{rec} = (+x\ -x\ +x\ -x)$.

(b) $\phi_1 = (+y\ -y)$, $\phi_2 = \phi_3 = \phi_5 = \phi_6 = \phi_{S3E} = (+x)$, $\phi_4 = (+x\ +x\ -x\ -x$ [A] / $-y\ -y\ +y\ +y$ [B]), $\phi_{rec} = (+x\ -x\ +x\ -x)$.

(c) $\phi_1 = (+y\ -y)$, $\phi_2 = \phi_3 = \phi_5 = \phi_{S3E} = (+x)$, $\phi_4 = (+x\ +x\ -x\ -x$ [A] / $-y\ -y\ +y\ +y$ [B]), $\phi_6 = -\phi_7 =$ $(+y\ -y$ [A] / $+x\ -x$ [B]) $\phi_{rec} = (+x\ -x\ +x\ -x)$.

(d) $\phi_1 = (+y\ -y)$, $\phi_2 = \phi_3 = \phi_5 = \phi_{S3E} = (+x)$, $\phi_4 = (+x\ +x\ -x\ -x$ [A] / $-y\ -y\ +y\ +y$ [B]), $\phi_6 = -\phi_7 =$ $(+y\ -y)$ $\phi_{rec} = (+x\ -x\ +x\ -x)$.

Pulse sequences in Bruker (Avance III) format are available to download at:
http://www2.warwick.ac.uk/fac/sci/chemistry/research/lewandowski/lewandowskigroup/goodies/

**Table S4.** Extended model free (EMF) analysis of $^{15}N$ & $^{13}C'$ relaxation in crystalline [U-$^{13}C$,$^{15}N$]GB1 (data plotted in Fig. 5 in the manuscript). Fitted data include $^{15}N$ $R_1$ and $R_{1\rho}$ at 600 MHz, 850 MHz, $^{13}C'$ $R_1$ and $R_{1\rho}$ at 600 MHz and 850 MHz and NH dipolar order parameters[6]. # indicates peptide plane number following the numberings of the amide nitrogens.

| # | $S_s^2$ | error | $\tau_s$ (ns) | error | $S_f^2$ | error | $\tau_f$ (ps) | error | $\chi^2$ |
|---|---|---|---|---|---|---|---|---|---|
| 3 | 0.995 | 3.17E-04 | 428 | 6 | 0.790 | 0.00149 | 48 | 4 | 145.3 |
| 4 | 0.997 | 4.28E-04 | 399 | 42 | 0.782 | 3.47E-04 | 13 | 4 | 93.3 |
| 5 | 0.996 | 2.97E-04 | 405 | 18 | 0.714 | 3.03E-04 | 24 | 3 | 90.2 |
| 6 | 0.998 | 0.00576 | 421 | 213 | 0.771 | 0.00452 | 18 | 5 | 42.0 |
| 7 | 0.999 | 0.00179 | 526 | 182 | 0.801 | 0.00146 | 15 | 3 | 27.2 |
| 8 | 0.998 | 0.0156 | 386 | 390 | 0.832 | 0.0133 | 21 | 5 | 41.8 |
| 9 | 0.997 | 3.03E-04 | 458 | 20 | 0.783 | 3.41E-04 | 33 | 4 | 203.8 |
| 10 | 0.986 | 0.00278 | 205 | 45 | 0.750 | 0.00446 | 82 | 8 | 36.0 |
| 11 | 0.990 | 5.09E-04 | 445 | 5 | 0.719 | 6.01E-04 | 45 | 3 | 73.7 |
| 13 | 0.997 | 2.52E-04 | 420 | 20 | 0.813 | 3.58E-04 | 33 | 7 | 92.2 |
| 14 | 0.994 | 4.39E-04 | 429 | 9 | 0.755 | 4.81E-04 | 34 | 3 | 211.5 |
| 15 | 0.997 | 5.28E-04 | 400 | 33 | 0.773 | 6.64E-04 | 39 | 6 | 30.2 |
| 16 | 0.996 | 3.58E-04 | 401 | 20 | 0.817 | 0.00196 | 60 | 8 | 127.9 |
| 17 | 0.994 | 0.00587 | 572 | 3430 | 0.776 | 0.00482 | 69 | 11 | 57.5 |
| 18 | 0.989 | 0.00163 | 324 | 48 | 0.763 | 0.00308 | 65 | 8 | 97.2 |
| 20 | 0.995 | 7.03E-04 | 563 | 77 | 0.664 | 0.00111 | 47 | 3 | 87.4 |
| 21 | 0.999 | 0.00202 | 5200 | 13800 | 0.710 | 0.00146 | 28 | 4 | 24.9 |
| 22 | 0.996 | 0.00445 | 669 | 4500 | 0.733 | 0.00345 | 53 | 8 | 17.1 |
| 23 | 0.997 | 3.96E-04 | 405 | 13 | 0.798 | 0.00197 | 65 | 7 | 78.8 |
| 25 | 0.993 | 6.84E-04 | 431 | 15 | 0.766 | 7.35E-04 | 38 | 8 | 55.4 |
| 26 | 0.997 | 2.33E-04 | 452 | 8 | 0.783 | 4.59E-04 | 37 | 7 | 109.7 |
| 27 | 0.997 | 0.0157 | 366 | 242 | 0.752 | 0.0122 | 18 | 7 | 78.0 |
| 28 | 0.997 | 4.03E-04 | 455 | 27 | 0.782 | 3.39E-04 | 24 | 4 | 46.2 |
| 31 | 0.998 | 3.30E-04 | 500 | 55 | 0.802 | 2.67E-04 | 9 | 4 | 22.5 |
| 33 | 0.998 | 2.43E-04 | 462 | 24 | 0.782 | 1.92E-04 | 11 | 5 | 55.1 |
| 34 | 0.998 | 2.81E-04 | 451 | 22 | 0.812 | 2.30E-04 | 10 | 5 | 102.1 |
| 35 | 0.998 | 0.00871 | 415 | 208 | 0.781 | 0.00699 | 19 | 7 | 32.7 |
| 37 | 0.996 | 5.45E-04 | 423 | 38 | 0.773 | 4.68E-04 | 24 | 5 | 94.0 |
| 38 | 0.996 | 4.21E-04 | 400 | 35 | 0.773 | 4.39E-04 | 26 | 5 | 110.6 |

| | $S_s^2$ | error | $\tau_s$ (s) | error | $S_f^2$ | error | $\tau_f$ (s) | error | $\chi^2$ |
|---|---|---|---|---|---|---|---|---|---|
| 39 | 0.988 | 0.0414 | 299 | 233 | 0.780 | 0.0349 | 29 | 11 | 38.4 |

| | | | | | | | | | |
|---|---|---|---|---|---|---|---|---|---|
| 40 | 0.991 | 0.00114 | 360 | 41 | 0.660 | 0.00252 | 100 | 11 | 41.9 |
| 41 | 0.860 | 0.147 | 31 | 19400 | 0.604 | 0.0953 | 92 | 13 | 31.4 |
| 42 | 0.933 | 0.0408 | 24 | 29700 | 0.771 | 0.0329 | 53 | 10 | 12.6 |
| 43 | 0.996 | 0.00552 | 376 | 126 | 0.783 | 0.00444 | 23 | 8 | 33.4 |
| 44 | 0.994 | 7.44E-04 | 416 | 38 | 0.805 | 6.29E-04 | 22 | 9 | 55.3 |
| 45 | 0.995 | 4.71E-04 | 429 | 17 | 0.784 | 4.31E-04 | 26 | 6 | 54.5 |
| 46 | 0.996 | 6.25E-04 | 333 | 46 | 0.819 | 0.0031 | 57 | 8 | 107.9 |
| 47 | 0.996 | 4.40E-04 | 430 | 14 | 0.844 | 9.14E-04 | 51 | 9 | 85.6 |
| 48 | 0.995 | 3.48E-04 | 414 | 13 | 0.766 | 0.00115 | 48 | 6 | 96.5 |
| 49 | 0.996 | 4.13E-04 | 412 | 18 | 0.724 | 4.41E-04 | 30 | 3 | 173.4 |
| 50 | 0.951 | 0.0419 | 26 | 175 | 0.799 | 0.0342 | 12 | 20 | 21.5 |
| 51 | 0.998 | 3.45E-04 | 538 | 67 | 0.771 | 2.69E-04 | 11 | 4 | 36.3 |
| 52 | 0.998 | 2.55E-04 | 430 | 16 | 0.792 | 2.38E-04 | 21 | 6 | 144.0 |
| 53 | 0.995 | 7.57E-04 | 423 | 50 | 0.754 | 5.77E-04 | 9 | 4 | 46.9 |
| 54 | 0.993 | 8.85E-04 | 506 | 53 | 0.805 | 7.20E-04 | 8 | 4 | 21.4 |
| 55 | 0.998 | 3.73E-04 | 451 | 59 | 0.792 | 3.16E-04 | 20 | 7 | 39.8 |

## References


(1) Lipari, G.; Szabo, A. *J. Am. Chem. Soc.* **1982**, *104*, 4546.
(2) Clore, G. M.; Szabo, A.; Bax, A.; Kay, L. E.; Driscoll, P. C.; Gronenborn, A. M. *J. Am. Chem. Soc.* **1990**, *112*, 4989.
(3) Chevelkov, V.; Zhuravleva, A. V.; Xue, Y.; Reif, B.; Skrynnikov, N. R. *J. Am. Chem. Soc.* **2007**, *129*, 12594.
(4) Chevelkov, V.; Fink, U.; Reif, B. *J. Biomol. NMR* **2009**, *45*, 197.
(5) Allard, P.; Hard, T. *J. Magn. Reson.* **1997**, *126*, 48.
(6) Wylie, B. J.; Sperling, L. J.; Nieuwkoop, A. J.; Franks, W. T.; Oldfield, E.; Rienstra, C. M. *P. Natl. Acad. Sci. USA* **2011**, *108*, 16974.
(7) Wylie, B. J.; Sperling, L. J.; Frericks, H. L.; Shah, G. J.; Franks, W. T.; Rienstra, C. M. *J. Am. Chem. Soc.* **2007**, *129*, 5318.
(8) Vandenhoogen, Y. T.; Treurniet, S. J.; Roelen, H. C. P. F.; Devroom, E.; Vandermarel, G. A.; Vanboom, J. H.; Altona, C. *Eur. J. Biochem.* **1988**, *171*, 155.
(9) Wishart, D. S.; Bigam, C. G.; Yao, J.; Abildgaard, F.; Dyson, H. J.; Oldfield, E.; Markley, J. L.; Sykes, B. D. *J. Biomol. NMR* **1995**, *6*, 135.
(10) Tollinger, M.; Sivertsen, A. C.; Meier, B. H.; Ernst, M.; Schanda, P. *J. Am. Chem. Soc.* **2012**, *134*, 14800.
(11) Ban, D.; Gossert, A. D.; Giller, K.; Becker, S.; Griesinger, C.; Lee, D. *J. Magn. Reson.* **2012**, *221*, 1.
(12) Kmiecik, S.; Gront, D.; Kolinski, A. *Bmc. Struct. Biol.* **2007**, *7*.
(13) Kurbanov, R.; Zinkevich, T.; Krushelnitsky, A. *J. Chem. Phys.* **2011**, *135*.
(14) Seewald, M. J.; Pichumani, K.; Stowell, C.; Tibbals, B. V.; Regan, L.; Stone, M. J. *Protein Sci.* **2000**, *9*, 1177.
(15) Shapiro, Y. E.; Meirovitch, E. *J. Phys. Chem. B* **2012**, *116*, 4056.
(16) Lewandowski, J. R.; Sein, J.; Sass, H. J.; Grzesiek, S.; Blackledge, M.; Emsley, L. *J. Am. Chem. Soc.* **2010**, *132*, 8252.
(17) Laage, S.; Lesage, A.; Emsley, L.; Bertini, I.; Felli, I. C.; Pierattelli, R.; Pintacuda, G. *J. Am. Chem. Soc.* **2009**, *131*, 10816.